P. E. Russell, Ed., *Microbeam Analysis—1989*

TARGET HEATING, PLASMA FORMATION, AND EXPANSION PROCESSES DURING LASER IONIZATION

Akos Vertes, Peter Juhasz, Laszlo Balazs, and Renaat Gijbels

Continuing experience with laser ionization and especially with laser microprobing in mass spectrometry of solids indicates extreme sensitivity of the resulting mass spectra toward many properties of both the target and the laser beam.[1] Our previous efforts in order to rationalize the details of laser-target interaction[2-5] led to the distinction of at least three different regimes of laser ionization. Each regime can be characterized by the deposited energy density in a single laser pulse: $(1 - R)\Phi\alpha\tau$, where Φ and τ are the irradiance and pulse length of the laser shot and α and R are the absorption and reflection coefficients of the material respectively.

Assuming moderately reflecting opaque targets and Q-switched lasers we can translate the distinctions into laser intensities.

a. *Low irradiance* ($\sim 10^5$-10^6 W/cm^2). Physical processes are dominated by surface heating and ionization of target particles. Mass transfer is negligible across the solid/vacuum interface. The mass spectrum contains a significant amount of molecular ions. This regime is favored in molecular-weight determination of organic molecules.

b. *Medium irradiance* ($\sim 10^7$-10^8 W/cm^2). Evaporation of the sample becomes non-negligible. Laser energy is absorbed both by the ionized vapor in front of the target and by the target itself. In this case complicated fragmentation and recombination processes and/or ion molecule reactions take place in the expanding plume. The mass spectra may provide structural information for organic samples.

c. *High irradiance* ($\sim 10^9$-10^{11} W/cm^2). The deposition of laser energy is governed by the strong absorption of the expanding plasma cloud created in the early phase of the laser pulse. Elemental lines are abundant in the mass spectra providing fair possibilities for trace analysis of inorganic solids.

In the following sections simple phenomenological models are presented and analyzed for the three cases. Temporal and raidal distributions of surface temperature are calculated for poor and good heat conductors. Low thermal conductivity yields a "hot spot" in the center of the beam and leads to slow decay of the excitation after the laser pulse. Elevated thermal conductivity leads to opposite effects: lower maximum temperature, larger lateral spread of the temperature rise, and faster decay following the pulse.

For medium and high irradiance, temperature profiles perpendicular to the surface are calculated. Medium-intensity pulses lead to mass transport across the sample surface and to a temperature maximum in the expanding plume. If the laser intensity is increased to the high-irradiance domain, the heating process exhibits two mechanisms. At the beginning of the laser pulse light is mainly absorbed by the solid. The temperature profiles are similar to the medium-irradiance case. As the density of the ionized plume increases in front of the sample, plasma absorption gains importance and reaches a point where it dominates all other forms of energy deposition. This leads to a sudden temperature rise accompanied by intense ionization.

The authors are at the Department of Chemistry, University of Antwerp, Universiteitsplein 1, B-2610 Wilrijk, Belgium.

Theoretical

1. *Low Irradiance.* As an approximation the complicated process of laser-target interaction is modeled as heating of a semi-infinite solid by a penetrating source:

$$\frac{\partial}{\partial t}[\rho e] = \nabla[\kappa\nabla(\rho e)] + (1 - R)\alpha\Phi \qquad (1)$$

where κ is the thermal diffusivity of the material (usually a nonlinear function of the temperature) and ρe denotes the energy density of the material. The TEM_{00} mode of the laser has a Gaussian radial distribution with beam radius w. The time dependence is replaced by a rectangular impulse composed of u(t) step functions:

$$\Phi(r,z,t) = \Phi_0 e^{-r^2/w^2} e^{-\alpha z}[u(t) - u(t - \tau)] \qquad (2)$$

For the sake of simplicity we assume constant thermal diffusivity here. If neither phase transformation nor mass transfer becomes significant and heat loss is negligible through the interface, this model can be solved to yield the surface temperature distribution[6] T(r,z = 0,t):

$$T(r,z=0,t) = \frac{(1 - R)\Phi_0\alpha}{\rho c_p}\int_0^{t^*} \frac{w^2 e^{-r^2/[w^2+4\kappa(t-t')]}}{w^2 + 4\kappa(t - t')} \cdot e^{\alpha^2\kappa(t-t')}\operatorname{erfc}(\alpha\sqrt{\kappa(t - t')})dt' \qquad (3)$$

where $t^* = \begin{cases} t, & \text{if } t \leq \tau \\ \tau, & \text{if } t > \tau \end{cases}$

and c_p denotes the specific heat of the material. Numerical evaluation of this formula

yields the temperature distribution on the surface during and after the laser pulse.

2. *Medium and High Irradiance.* If mass transfer across the surface is considerable we have to include all three conservation laws in the description. The one-dimensional form of mass, momentum, and energy conservation has the following form[3];

$$\frac{\partial}{\partial t}[\rho] = -\frac{\partial}{\partial z}[\rho v] \tag{4}$$

$$\frac{\partial}{\partial t}[\rho v] = -\frac{\partial}{\partial z}[p + \rho v^2] \tag{5}$$

$$\frac{\partial}{\partial t}[\rho(e + v^2/2)] = -\frac{\partial}{\partial z}\left[\rho v\left(e + \frac{p}{\rho} + \frac{v^2}{2}\right)\right] + (1 - R)\alpha\Phi \tag{6}$$

where v denotes the hydrodynamic velocity and p stands for the pressure. Since thermal conduction transports a negligible fraction of the energy, especially at high intensities, we omitted the corresponding term in Eq. (6) (cf. Eq. 1). The equations of conservation have to be complemented by the equation of state relating pressure to density and energy. From the ideal gas law, we have the well-known form

$$p = (1 + \eta)\rho kT/m \tag{7}$$

where η is the degree of ionization $\eta = \eta_i/\eta_{total}$, expressed by the number density ratio of ions and all particles; m denotes the mass of the particles. The internal energy density is related to the state variables:

$$\rho e = \frac{\rho}{m}\left[\frac{3}{2}(1 + \eta)kT + \eta I_p\right] \tag{8}$$

where I_p is the ionization potential.

To determine the degree of ionization, the Saha-Eggert equation was used with the customary simplifications:

$$\frac{\eta^2}{1 - \eta^2} = \frac{m}{\rho}\left(\frac{2\pi\kappa T m_e}{h^2}\right)^{3/2} e^{-I_p/(kT)} \tag{9}$$

where m_e denotes the mass of the electron.

The linear light absorption coefficient $\alpha(z,t)$ consists of two terms. The first accounts for the normal absorption α_0 of the solid without ionization; the second takes into account the absorption α_{pl} of the plasma cloud

$$\alpha(z,t) = \alpha_0(z,t) + \alpha_{pl}(z,t) \tag{10}$$

Finite-difference solution of this one-component, one-dimensional (1C-1D) model requires special techniques due to the abrupt changes caused by the laser pulse. Further details of the model and the solution techniques were described earlier.[3]

Results

At low irradiance radial distributions of surface temperature were calculated at various instances. The results for a nonreflecting strong absorber (R = 0; $\alpha = 2.7 \times 10^5$ cm^{-1}) are depicted in Fig. 1. The density and specific heat of the solid were $\rho = 8$ g/cm^3 and $c_p = 0.385$ J/gK, respectively. To emphasize the importance of a widely neglected factor in laser ionization studies, the behavior of a poor and a good heat conductor is demonstrated. In Fig. 1(a) we used $\kappa = 0.0195$ cm^2/s for low thermal conductivity; in Fig. 1(b) we set $\kappa = 0.195$ cm^2/s to represent a good heat conductor.

Dramatic differences can be observed in the surface temperature distributions for the two cases. The most significant are that the poor conductor is heated to much higher temperatures and retains elevated values for a longer time.

The temperature distribution perpendicular to the surface at the end of a moderate-intensity ruby laser pulse is shown in Fig. 2 on the basis of our 1C-1D model. The nonreflecting opaque sample (R = 0; $\alpha_0 = 10^3$ cm^{-1} had $\eta_{total} = 10^{22}$ cm^{-3} number density and consisted of $m = 4 \times 10^{-23}$ g particles. For the ionization potential I_p, a value of 12 eV was used. Although the solid had an absorption coefficient 270 times lower than the target of the low-intensity calculation, and although the irradiance was only less than an order of magnitude higher, we could observe stronger heating, especially in the plasma cloud in front of the sample.

The same target was exposed to a 100 times larger irradiance laser pulse in the next calculation. Temperature profiles at consecutive time stages are displayed in Fig. 3. Strong heating can be observed during the first quarter of the laser pulse (Figs. 3a and b), leading to almost complete ionization in the expanding plume. In the second half of the laser pulse the plasma absorption substantially outweighs the normal absorption. As a result a sudden change in the character of the temperature profiles can be observed. The plasma heats up inducing further ionization and that in turn increases the absorption. This positive feedback produces an extreme temperature rise and fast expansion of the plasma. Details of these processes are described in other papers.[3,5]

Conclusions

The large body of experimental observation on laser ionization of solids can be divided into categories according to the amount of deposited energy and the quantity of ablated material.

For low energy deposition and negligible mass transfer across the sample/vacuum interface, lateral distributions of surface temperature can be calculated. These results open the way to checking previous qualitative models based on the cross-sectional structure of the illuminated spot in laser ionization experiments.[7] On the basis of surface temperatures it also becomes possible to judge to what extent the temperature rise is responsible

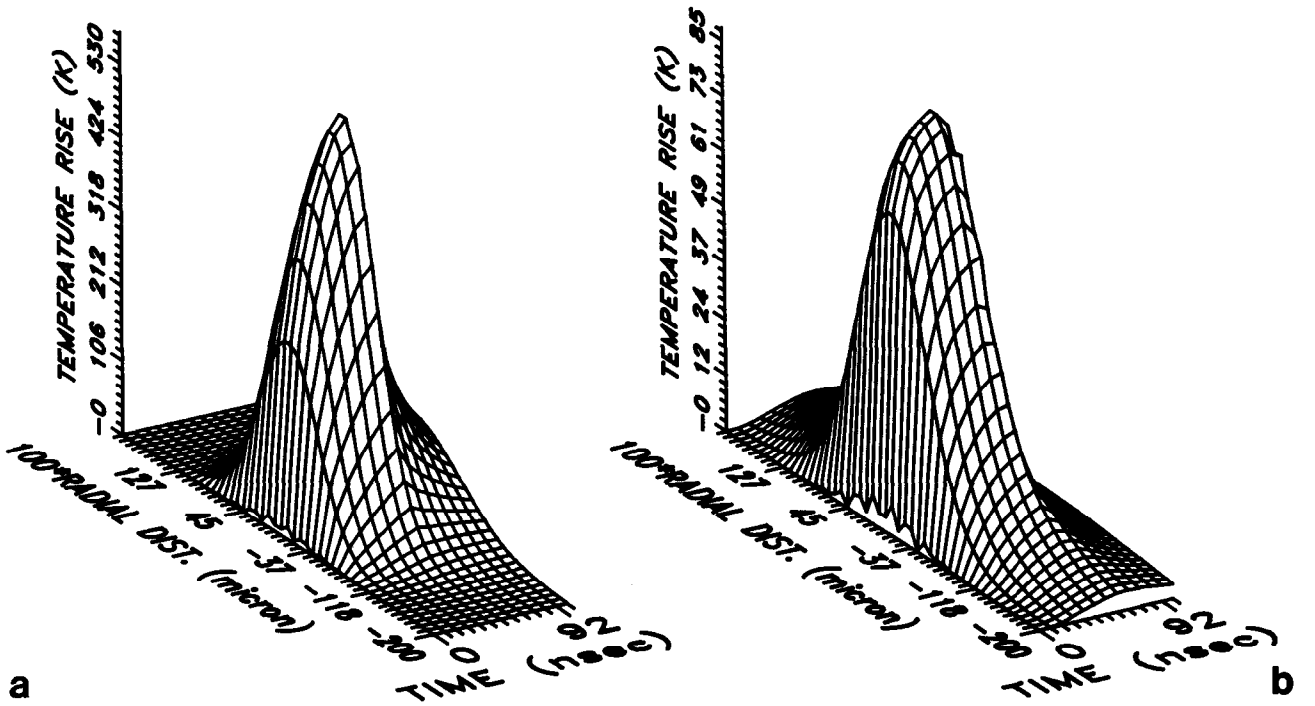

FIG. 1.--Surface temperature rise of strongly absorbing target due to low-power-density laser pulse ($\Phi_0 = 1.6 \times 10^6$ W/cm^2; $\tau = 50$ ns); beam radius is w = 0.5 μm. (a) Poor heat conductor, (b) good heat conductor.

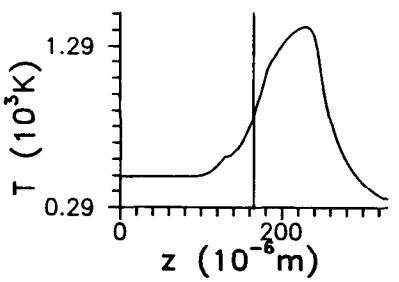

Fig. 2.--Heating opaque sample by moderate-intensity ruby laser pulse ($\Phi_0 = 10^7$ W/cm^2; $\tau = 50$ ns). Vertical line shows original position of solid (left)/vacuum (right) interface; light is arriving from vacuum side.

for ion formation. Other mechanisms such as multiphoton ionization or Coulomb repulsion can be compared to thermally induced processes.

Material transport across the sample surface is an important factor at medium and high energy deposition. In the medium range the emphasis from solid-phase light absorption shifts toward absorption by the plume. Temperature, density, velocity, and ionization degree profiles can be calculated perpendicular to the surface.[3] With irradiance increasing above a certain threshold (plasma ignition threshold[4]) the ionized plume absorbs heavily (shielding the surface from radiation) and reaches extremely high temperatures.

References

1. L. Van Vaeck, J. Bennett, W. Lauwers, A. Vertes, and R. Gijbels, "Laser microprobe mass spectrometry: Possibilities and limitations," *Microbeam Analysis--1988*, 351.

2. A. Vertes, P. Juhasz, P. Jani, and A. Czitrovszky, "Kinetic energy distribution of ions generated by laser ionization sources," *Int. J. Mass Spectr. Ion Proc.* 83: 45, 1988.

3. A. Vertes, P. Juhasz, M. De Wolf, and R. Gijbels, "The role of energy deposition processes in the understanding of laser microprobe analysis mechanisms," *Scanning Microscopy*, 2: 1853, 1988

4. A. Vertes, M. De Wolf, P. Juhasz, and R. Gijbels, "Threshold conditions of plasma ignition in laser ionization mass spectrometry of solids," *Anal. Chem.* (in press).

5. A. Vertes, P. Juhasz, M. De Wolf, and R. Gijbels, "Hydrodynamic modeling of laser ionization processes," *Int. J. Mass Spectr. Ion Proc.* (in press).

6. B. J. Bartholomeusz, "Thermal response of a laser-irradiated metal slab," *J. Appl. Phys.* 64: 3815, 1988.

7. D. M. Hercules, R. J. Day, K. Balasanmugam, T. A. Dang, and C. P. Li, "Laser microprobe mass spectrometry: 2. Applications to structural analysis," *Anal. Chem.* 54: 280A, 1982.

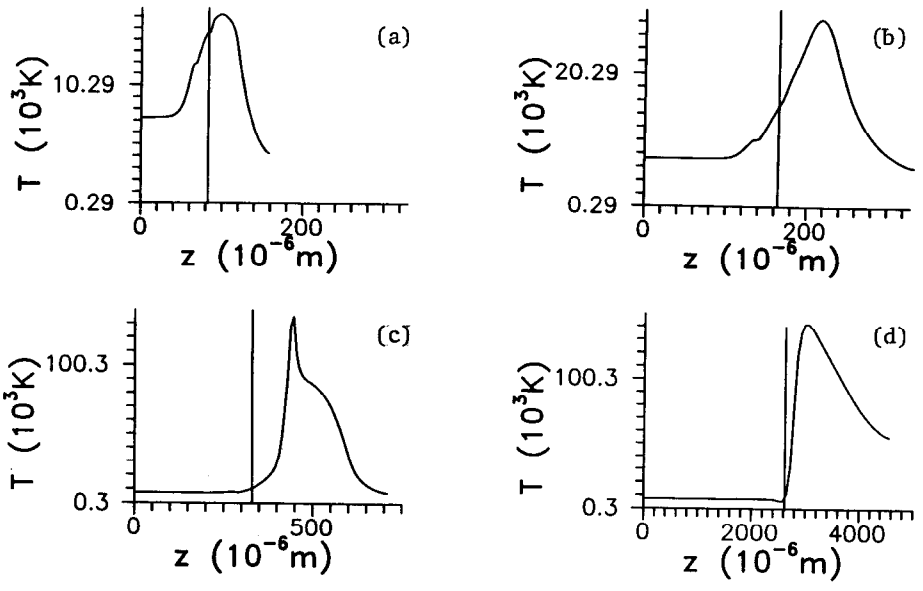

FIG. 3.--Time development of temperature profile during high-intensity ruby laser pulse ($\Phi_0 = 10^9$ W/cm^2; $\tau = 50$ ns) hitting same target as in Fig. 2. (a) after 7 ns, (b) 12 ns, (c) 21 ns, (d) 50 ns.